ELSEVIER

Astroparticle Physics 14 (2000) 141–152

Astroparticle Physics

www.elsevier.nl/locate/astropart

Prospects of scintillating crystal detector in low-energy low-background experiments

H.T. Wong [a,*], J. Li [b], C.Y. Chang [c], C.C. Chang [c], C.P. Chen [a], W.P. Lai [a], H.B. Li [d], Y. Liu [b], J.G. Lu [b], Z.P. Mao [b], S.C. Wang [a]

[a] *Institute of Physics, Academia Sinica, Nankang, Taipei 11529, Taiwan*
[b] *Institute of High Energy Physics, Beijing 100039, China*
[c] *Department of Physics, University of Maryland, MD, USA*
[d] *Department of Physics, National Taiwan University, Taipei 10617, Taiwan*

Received 7 October 1999; revised 17 January 2000; accepted 27 January 2000

Abstract

A scintillating crystal detector offers potential advantages in low-energy (keV–MeV range) low-background experiments for particle physics and astrophysics. The merits are discussed using CsI(Tl) crystal as illustrations. The various physics topics, which can be pursued with this detector technology, are summarized. A conceptual design for a generic detector is presented.

PACS: 14.60.Pq; 95.35.+d; 29.40.Mc
Keywords: Neutrinos; Dark matter; Scintillation detector

1. Introduction

Scintillating crystal detectors [1] [1] have been widely used as electromagnetic calorimeters in high energy physics [2], [2] as well as in medical and security imaging and in the oil-extraction industry. They have also been adopted for non-accelerator experiments, notably NaI(Tl) detectors are already used in dark matter searches [3–8], producing some of the most sensitive results.

Several characteristic properties make crystal scintillator an attractive detector option for low-energy (keV to MeV range) low-background experiments. Subsequent sections of this article will bring out the potential advantages of this approach and some of the physics topics well suited to be investigated by this detector technology. The characteristic performance of the CsI(Tl) crystal are used as illustrations. A generic design to exploit these merits in a realistic experiment is discussed in Section 4.

* Corresponding author. Tel.: +886-2-2789-9682; fax: +886-2-2788-9828.
E-mail address: htwong@phys.sinica.edu.tw (H.T. Wong).

[1] For a recent review on the crystal scintillator see eg., Ref. [1] and references therein.

[2] For a recent review on the applications of crystal scintillator in particle physics, see e.g., Ref. [2].

0927-6505/00/$ - see front matter
PII: S0927-6505(00)00108-0

2. Motivations and merits

2.1. Nuclear physics

The physics at the keV–MeV range can depend critically on the choice of isotopes as the interaction targets. The nuclear structure determines the interaction cross-sections, detection threshold, as well as experimental signatures like spatial or temporal correlations.

The deployment of target with a large mass for low energy experiments usually requires that the target is an active detector. There are only a few detector technologies, which accommodates a wide range of possible nuclei. The choice is even more limited when the potentials and possibilities to scale-up to a massive (tons or more) detector have to be taken into account. The two most prominent candidate techniques are loaded liquid scintillator and crystal scintillator.

2.2. Existing experience and potential spin-offs

Large target-mass requirement is always a challenge to low count rate experiments. From the big electro-magnetic calorimeters in high energy physics, there is much experience in producing and operating 50-ton-range crystal calorimeters. The technology is proven to be stable and robust at the harsh accelerator environment. Indeed, the present broad applications and affordable price range for crystals like CsI(Tl) and BGO are driven mostly by the demand and development from high energy physics experiments. Therefore, it is possible that construction of a big scintillating crystal detector for low-energy experiments will also lead to the maturity of a new technology with potential spin-offs in other areas.

2.3. Intrinsic properties

Some of the properties of crystal scintillators make them favorable candidates to be adopted for studying low-energy low-background experiments *relative* to the various other proposed detector schemes. Although different crystals do have different characteristic performance parameters, the merits of this detector approach are discussed below using CsI(Tl) as an illustration.

The characteristic properties of CsI(Tl) [9,10], together with a few other common crystals as well as liquid and plastic scintillators, are summarized and compared in Table 1. The selection of CsI(Tl) is due to the fact that it is a commonly used and relatively inexpensive crystal scintillator produced in large quantities and with many examples of successful operation as 50-ton-range electro-magnetic calorimeters, as in all the B-factory detectors currently under operation. Unlike NaI(Tl), it is only slightly hygroscopic and can operate stably for a long time without the need for a hermetic seal (based on experiences from high energy physics experiments). This minimizes the use of passive materials at the target volume, which, as explained below, is crucial to allow the merits of this detector technique for low-energy low-background experiments to be fully exploited.

Table 1
Characteristic properties of the common crystal scintillators and their comparison with typical liquid and plastic scintillators

Properties	CsI(Tl)	NaI(Tl)	BGO	Liquid	Plastic
Density ($g\,cm^{-3}$)	4.51	3.67	7.13	0.9	1.0
Relative light yield	0.45	1.00[a]	0.15	0.4	0.35
Radiation length (cm)	1.85	2.59	1.12	~45	~45
dE/dx for MIP ($MeV\,cm^{-1}$)	5.6	4.8	9.2	1.8	1.9
Emission peak (nm)	565	410	480	425	425
Decay time (ns)	1000	230	300	2	2
Refractive index	1.80	1.85	2.15	1.5	1.6
Hygroscopic	Slightly	Yes	No	No	No

[a] Typical light yield for NaI(Tl) is about 40 000 photons per MeV.

2.3.1. Solid and compact detector

Crystal scintillators usually have high density and are made up of high-Z isotopes. Therefore, a massive (tens of tons) detector can still be very compact (scale of several m^3), such that external shielding configurations can be made more efficient and cost effective. The compact dimension also favors applications, where artificial neutrino sources are used thereby allowing efficient exposure of the target materials to the source.

A solid detector can also prevent radioactive radon gas from diffusing into the inner fiducial volume from the external surfaces. This is a major concern for target based on gaseous or liquid detectors. Special procedures are still necessary to minimize the radon contaminations on crystal surfaces, as noted in Sections 2.3.3 and 4.

2.3.2. Efficient active veto

The attenuation effects of CsI(Tl) to γ-rays of different energy, together with those of the water and liquid scintillator (a generic CH_2 compound with density 0.9 $g\,cm^{-3}$) [11], are depicted in Fig. 1. In the region between 500 keV and around 3 MeV, Compton scattering (which varies with the atomic number Z) is the main process, and therefore, the attenuation effects of CsI(Tl) are only enhanced by the density ratio, relative to H_2O and CH_2. Above several MeV, the pair production (varying as Z^2) takes over making the high-Z CsI(Tl) more efficient. This is the reason of choosing this crystal as electromagnetic calorimeters. In the low energy region below 500 keV, photo-electric effects (varying as Z^5) dominates overwhelmingly. For instance, the attenuation lengths for a 100 keV γ-ray are 0.12 and 6.7 cm, respectively, for CsI(Tl) and CH_2, i.e., 1 cm of CsI(Tl) is equivalent to eight attenuation lengths, and 10 cm of CsI(Tl) has the same attenuating power as 5.6 m of liquid scintillator at this low energy. Most crystal scintillators, having high-Z isotopes, share this merit.

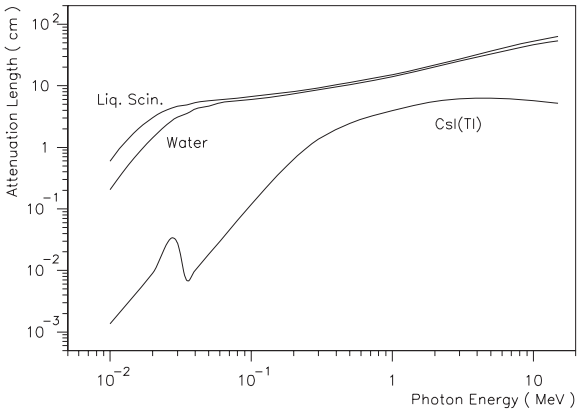

Fig. 1. The attenuation length, as defined by interactions that lead to a loss of energy in the media, for photons at different energies, for CsI(Tl), water, and liquid scintillator.

2.3.3. Focus only on internal background

Given the large attenuating effects on low energy photons, crystal detectors can provide a unique advantage to the background suppression in low energy experiments – that external γ-background are highly suppressed such that practically all γ-background originates internally IF (1) a three-dimensional fiducial volume can be defined, and (2) a housing-free design with minimal passive materials can be realized.

For non-hygroscopic crystals like CsI(Tl) or BGO, where a hermetic seal system is not needed for their operation, "*internal*" would include only two materials: the crystal itself and the surface wrapping or coating materials. Teflon wrapping sheets are most commonly used, while there is an interesting new development with sol–gel coating, which can be as thin as a few microns [12]. Teflon is known to have very high radio-purity (typically better than the ppb level for the ^{238}U and ^{232}Th series) [13].

The suppression of radon contamination to the inner fiducial volume requires special but standard procedures. Crystal surfaces as well as the Teflon wrapping sheets should be cleaned before wrapping, preferably in a nitrogen-filled glove box. The detector modules should be covered and protected by an additional surface (like aluminum foils), which will be removed only at the time of installation. The whole detector should be installed and operate in an air-tight box filled with clean nitrogen.

As a result, the experimental challenges and hurdles become focussed on to two distinct aspects:

1. *backgroundwise*: the control and understanding of the internal purity of the crystal target itself;
2. *detectorwise*: the realization of a detector design giving good position resolutions and with as low a threshold as possible.

Accordingly, the difficulties for external gamma-background control can be alleviated at the expense of additional detector requirements.

The internal background can be due to contaminations of naturally occurring isotopes (^{238}U and ^{232}Th series, ^{40}K), long-lived fission products and cosmic ray-induced unstable nuclei. The background due to external γs, such as those from the readout device, electronics components, construction materials, or radon contamination on the outer surfaces, can thus be attenuated and vetoed by the outer active volume. The background can also originate externally from cosmic-ray induced neutrons, which have little attenuation with high-Z nuclei. Their effects, however, can be minimized by a cosmic veto and by operating the experiment underground.

Hygroscopic crystals like NaI(Tl) are housed in containers as hermetic seal. The containers, usually made of oxygen-free copper for low background application, can be made to have high radiopurity. However, it is still an inactive material with high cross-sections for photons. Consequently, it is possible that high energy photons (which have less attenuation in the crystal) can penetrate into the fiducial volume, undergo Compton scatterings at the passive container, and deposit only low energy at the crystal detector itself. Therefore, the adoption of non-hygroscopic crystals (i.e., a housing-free set-up) is essential to exploit the full power of this merit – that there is big suppression for external photons at low energies (<500 keV) to get into fiducial volume or for those at high energies (>MeV) to get into fiducial volume but deposit only 100 keV of visible signals.

The background count rate will be stable and not affected by external parameters if the dominant contributions are from internal contaminations. Therefore, this detector technique can provide additional desirable feature in applications requiring delicate comparison and subtraction of data taken at different periods (such as reaction ON/OFF, annual modulation, day/night effects). The light yield for scintillating crystals is usually temperature-dependent, and therefore a good calibration scheme and temperature-control of the detector region is crucial to realize these subtraction procedures.

It should be stressed that an experimental design, which provides the definition of a three-dimensional fiducial volume is essential to allow this large suppression of the external gamma background. The extent to which this can be achieved in a realistic detector set-up will depend on the specific crystal properties (particularly the light yield), and the energy range of interest. This will be discussed further in Sections 4 and 5.

2.3.4. Good energy resolution and modularity

Light yield of typical crystal scintillators are comparable to those of liquid and plastic scintillators. However, the modular size are smaller, whereas the refractive index higher, leading to more efficient light transmission and collection. The high gamma attenuation also allows full γ-energy deposition. Consequently, crystal scintillators have typically better energy resolution and lower detection threshold, both of which are necessary for low-energy measurements. The high γ-rays capture efficiency, together with the good resolution to measure them as energy-peaks, can provide important diagnostic tools for understanding the physical processes and background of the system. For instance, by measuring the γ-peaks due to ^{40}K, ^{60}Co and ^{137}Cs, their associated β-background can be accurately accounted for and subtracted off.

The good modularity also enhances background suppression, since the interesting signals for most applications are single-site events. Most background from internal radioactivity come as $\beta + \gamma$s in coincidence (like decays of ^{214}Bi and ^{208}Tl from the ^{238}U and ^{232}Th series, respectively) and hence, will produce multiple hits with high probability. Similarly, neutron capture events by the target isotopes manifest as (n, γ) interactions, giving rise to a γ-burst of multiple hits with known total energy. The neutron capture rate can therefore be measured, such that the background due to subsequent decays of the unstable daughter nuclei can be subtracted off.

2.3.5. Possibility of pulse shape discrimination

Crystals such as CsI(Tl) and NaI(Tl) have superb pulse shape discrimination (PSD) properties [14,15] to differentiate γ/e events from those due to heavily ionizing particles like αs, which have a faster fall time. Fig. 2 depicts typical PSD between α/γ in CsI(Tl) with the "partial charge vs total charge" method [16,17], demonstrating excellent separation. The PSD capabilities provide powerful handle to tag and study those background channels involving alpha emission, such as those from the ^{238}U and ^{232}Th decay chains.

2.3.6. High sensitivity to U/Th cascades

Unlike in liquid scintillators, αs are only slightly quenched in their light output in crystals like CsI(Tl) and NaI(Tl). The exact quenching ratio depends on the Tl concentration and the measurement parameters such as shaping time – for full integration of the signals, the quenching is about 50% [9,10]. Therefore, some of the αs emitted from the uranium and thorium series are above 3 MeV. This is beyond the end-point for natural radioactivity (2.61 MeV) and hence, the peak signatures are easy to detect among the flat background. In comparison, the electron-equivalence light yield for several MeV αs in liquid scintillators is typically less than 10% of their kinetic energy, making the signals well below the natural end-point and therefore more difficult to detect.

A crystal contaminated by uranium or thorium would therefore give rise to multiple peaks above 3 MeV, as reported in Ref. [18,19] in the case of CsI(Tl). Shown in Fig. 3 is the background spectrum from a 5-kg CsI(Tl) crystal kept in a 5 cm of lead shielding with cosmic veto in a typical sea-level laboratory. The absence of multiple peaks above 3 MeV suggests a ^{238}U and ^{232}Th concentration of less than the 10^{-12} g/g level, assuming that the decay chains are in equilibrium. All the peaks and structures in the spectrum can be explained by ambient radioactivity or by (n,γ) interactions at the crystal and shielding materials. This simple yet effective measurement for crystal scintillator can be compared to the complicated schemes requiring elaborate underground facilities for liquid scintillator [20]. A typical level achievable by the photon-counting method with a low-background germanium is only 10^{-9} g/g [13].

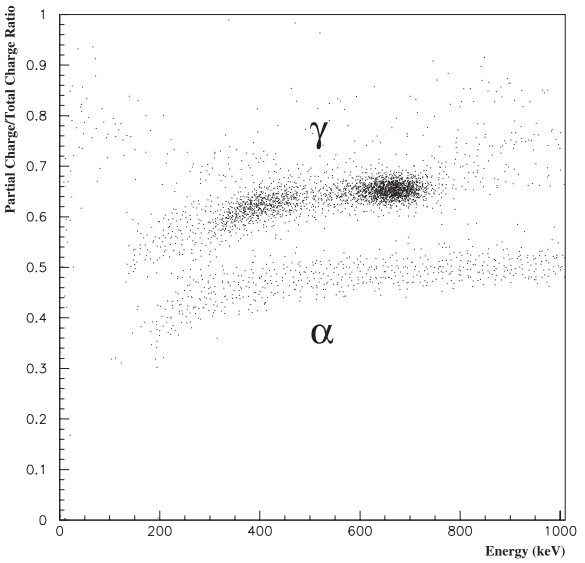

Fig. 2. The partial charge/total charge ratio in a CsI(Tl) crystal as a function of energy, showing excellent pulse shape discrimination capabilities to differentiate events due to αs and γs. The γ-events are due to a ^{137}Cs source, showing peaks at the full-energy and Compton edge regions. The α-events are from the low-energy tails of an ^{241}Am source placed on the surface of the crystal.

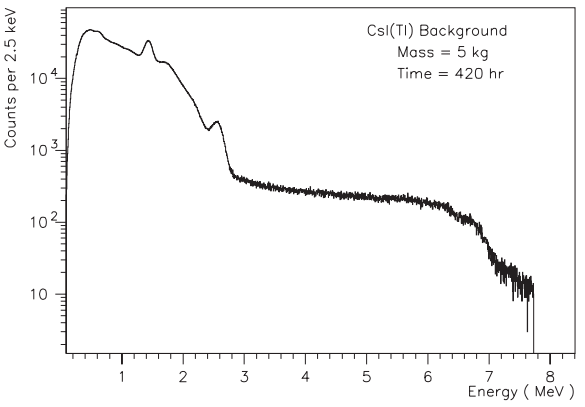

Fig. 3. Measured background spectrum of a 5 kg CsI(Tl) under lead shieldings and cosmic-ray veto. The absence of peaks above 3 MeV provides sensitive limits to contaminations of ^{238}U and ^{232}Th decay chains in equilibrium.

The sensitivities can be pushed further by taking the measurement underground (the flat background above 3 MeV are due to cosmic-ray induced neutrons, which undergo (n,γ) when captured by the crystal or the shielding materials), and by exploiting the PSD characteristics of the crystal. In addition, by carefully studying the timing and energy correlations among the αs, one can obtain precise information on the radioactive contaminants in the cases, where the ^{238}U and ^{232}Th decay series are not in equilibrium, so that the associated β/γ background can be accounted accurately. For instance, some dark matter experiments with NaI(Tl) [3–6] reported trace contaminations (range of 10^{-18}–10^{-19} g/g) of ^{210}Pb in the detector, based on peaks from γs of 46.5 keV and from αs of 5.4 MeV. Accordingly, β-decays from ^{210}Bi can be subtracted off from the signal.

3. Potential applications

Several areas of low energy particle physics, where the crystal scintillator technique may be applicable are surveyed in this section.

3.1. Neutrino–electron scattering at low energy

Scatterings of the $(\nu_e e)$ and $(\bar{\nu}_e e)$ give information on the electro-weak parameters (g_V, g_A, and $\sin^2\theta_W$), and are sensitive to small neutrino magnetic moments (μ_ν) [21]. They are two of the most realistic systems, where the interference effects between Z and W exchanges can be studied [22].

The goal of future experiments will be to push the detection threshold as low as possible to enhance the sensitivities in the magnetic moment search. Using reactor neutrinos as source, an experiment based on a gaseous time projection chamber with CF_4 [23,24] is now operational. Another experiment using CsI(Tl) is being built [25], with the goal of achieving a threshold of 100 keV. A project with NaI(Tl) detector at an underground site and using an artificial neutrino source has also been discussed [26].

3.2. Neutral current excitation on nuclei

Neutral current excitation (NCEX) on nuclei by neutrinos has been observed only in the case of ^{12}C [27] with 30 MeV neutrinos. Excitations with lower energies using reactor neutrinos have been studied theoretically [28,29] but not observed.

Crystal scintillators, having good γ resolution and capture efficiency, are suitable to study these processes, where the experimental signatures are peaks in the energy spectra with characteristic energies. Realistic experiments can be based on using the crystal isotopes as active targets, like ^{133}Cs and ^{127}I in CsI(Tl) or ^{6}Li, ^{7}Li and ^{127}I in LiI(Eu). The ^{7}Li case, with a γ-energy of 480 keV, has particularly large cross-sections. Alternatively, a compact passive boron-rich target like B_4C can be inserted into an array of CsI(Tl) detector modules [25]. There are theoretical work [30–32] suggesting that the NCEX cross-sections on ^{10}B and ^{11}B are sensitive to the axial isoscalar component of NC interactions and the strange quark content of the nucleon.

3.3. Dark matter searches

Direct searches of weakly interacting massive particles (WIMP) [33] [3] are based on looking for the low-energy (few keV) nuclear recoil signatures when they interact with the nuclei. Crystal scintillators may offer an appropriate detector technique for these studies from their PSD capabilities, as well as being a matured technology, where a large target mass is possible. The cross-sections depend on specific isotopes [34,35], based on their nuclear matrix elements and spin states.

The NaI(Tl) crystal detectors [3–6] are already used in WIMP searches. Up to the scale of 100 kg target mass has been deployed [7,8], producing some of the most sensitive results. Other projects on CaF_2(Eu) [36,37] and CsI(Tl) [38] are also pursued. In addition, searches have been per-

[3] For a recent review, see, e.g., Ref. [33].

formed [39,40] with the WIMP-nuclei inelastic scattering [41,42] giving rise to NCEX.

For crystal detectors, where a three-dimensional fiducial volume with minimal passive materials can be defined, there is no background due to external γs at this low energy. Internal β background is suppressed by the spectral distribution at this very low energy range. For instance, less than 3×10^{-4} of the β-decays in ^{40}K (end-point 1.3 MeV), give rise to events below 10 keV. However, achieving a three-dimensional fiducial volume definition will be more difficult at these low energies, as elaborated in Section 5.

3.4. Low energy solar neutrinos

The goal of future solar neutrino experiments [43] [4] will be to measure the low energy (pp and ^{7}Be) solar neutrino spectrum. Charged- (CC) and neutral-current (NC) on nuclei are attractive detection channels besides neutrino–electron scattering. The CC mode can provide a direct measurement of the ν_e-spectrum from the sun without the convolutions necessary for the ν–e channels, whereas the NC mode can provide a solar model independent cross-check. Crystal scintillators are possible means to realize detectors based on the CC and NC interactions.

Previously, crystals with indium has been investigated [44–47] for a $\nu_\odot$-detector with ^{115}In as target, which can provide a distinct temporally and spatially correlated triple coincidence signature. Recently, the crystals LiI(Eu) [48] and Gd_2SiO_5(Ce) (GSO) [49,50] are being considered. The attractive features are that LiI(Eu) have large ν_eN–CC cross-sections for both ^{7}Li and ^{127}I, and ν_eN–NC ($E_\gamma = 480$ keV) for ^{7}Li, while ^{160}Gd in GSO can provide another time-delay signature for background suppression and for tagging the flavor-specific ν_eN–CC reactions. The primary experimental challenge is the requirements of extremely low background level due to the small signal rate.

[4] For a recent review, see e.g., Ref. [43].

3.5. Double beta decay

The energy range of interest for the search of neutrino-less double beta decay [51] is mostly above 1 MeV, and hence some of the merits for crystal scintillators discussed in Section 2 relative to the other techniques are no longer applicable. We mention for the scale of completeness that there are efforts on ^{115}Cd with $CdWO_4$ [52] and on ^{160}Gd with GSO [53,54] crystals.

4. Generic detector design

To fully exploit the advantageous features discussed in Section 2, the design of a scintillating crystal detector for low-energy low-background experiments should enable the definition of a fiducial volume with a surrounding active 4π-veto.

Displayed in Fig. 4 is a generic conceptual design, where such a detector can be realized. The detector design is based on an experiment being constructed [25], which, in its first phase, will study

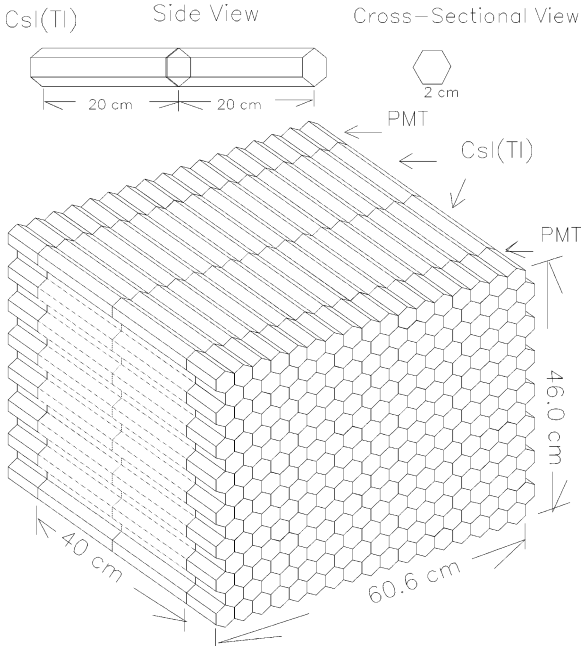

Fig. 4. The schematic design of a generic scintillating crystal detector.

low energy neutrino–electron scattering from reactor neutrinos using CsI(Tl) as target. The listed dimensions are for this particular experiment. The dimensions for other applications will naturally depend on the optimization based on the specific detector performance and requirements.

As shown in Fig. 4, one CsI(Tl) crystal unit consists of a hexagonal-shaped cross-section with a 2 cm side and a length 20 cm, giving a mass of 0.94 kg. Two such units are glued optically at one end to form a module, where the light output from both ends are read out by photo-detectors. Photomultipliers (PMTs) will be used for the experiment though solid-state photo-detectors like photodiodes or avalanche photo-diodes are also possibilities for other applications. The modular design enables the detector to be constructed in stages. Fig. 4 shows a design with a 17×15 matrix giving a total mass of 480 kg.

The cleaning and wrapping procedures to minimize radon contamination to the crystal surfaces noted in Section 2.3.3 will be adopted. The detector will operate inside an air-tight box filled with dry nitrogen. The box itself will in turn be inside a nitrogen air-bag. The compact dimensions of the inner target detector allow a more elaborate and cost-effective shielding design. External to the air-bag are the typical shielding configurations: from outside inwards plastic scintillators for cosmic-ray veto, 15 cm of lead, 5 cm of steel, 25 cm of boron-loaded polyethylene, and 5 cm of copper. Potassium-free PMT glass window as well as other high radiopurity materials will be used near the target region.

The energy deposited can be derived from the sum of the two PMT output ($Q_{\rm tot} = Q_1 + Q_2$) after their gains are normalized, whereas the longitudinal position can be obtained from their difference in the form of $R = (Q_1 - Q_2)/(Q_1 + Q_2)$. The variation of Q_1, Q_2 and $Q_{\rm tot}$ along the crystal length are displayed in Fig. 5. The error bars denote the width of the photo-peaks of a ^{137}Cs source. The discontinuity in the middle is due to the optical mismatch between the interface glue ($n = 1.5$) and the crystal ($n = 1.8$). It can be seen that $Q_{\rm tot}$ is independent of the position, and the resolution at 660 keV is about 10%. The detection threshold (where signals are measured at both PMTs) is <20 keV.

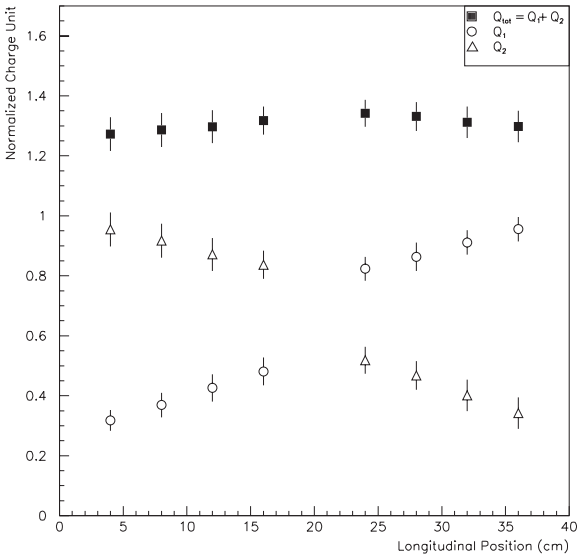

Fig. 5. The measured variations of Q_1, Q_2 and $Q_{\rm tot} = Q_1 + Q_2$ along the longitudinal position of the crystal module. The charge unit is normalized to unity for both Q_1 and Q_2 at their respective ends. The error bars denote the width of the photo-peaks due to a ^{137}Cs source.

The variation of R along the crystal length is depicted in Fig. 6. The ratio of the RMS errors in R relative to the slope gives the longitudinal position resolution. Its variation as a function of energy, obtained from measurements with γ-sources of different energies, is displayed in Fig. 7, showing a resolution of <2 and 4 cm at 660 and 100 keV, respectively. Only an upper limit of 2 cm on the resolution can be justified above 350 keV due to (a) finite collimator size for the calibration sources, and (b) the event-sites of γ-interactions (mostly multiple Compton scattering) being less localized at higher energies. It can be seen that a three-dimensional fiducial volume can be defined above 50 keV, where the definitions can be optimized for different energy ranges. For instance, a 10-cm active veto length will give a suppression factor of 5×10^{-3} to external photons of 100 keV. The fiducial volume consists only of the crystal itself and the teflon wrapping sheets, typically in a mass ratio of 1000:1.

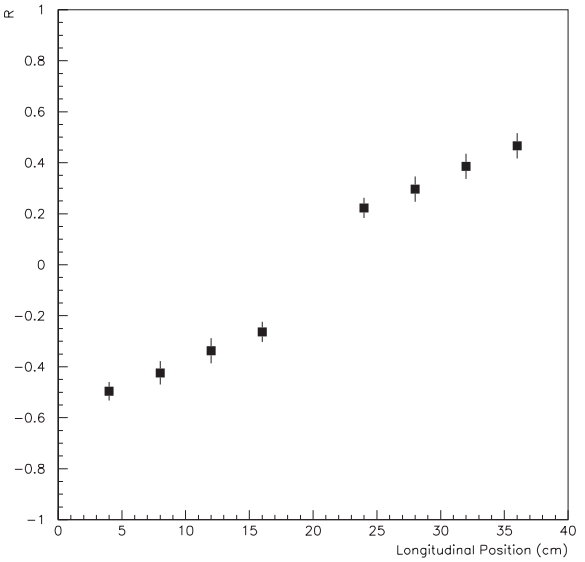

Fig. 6. The variation of $R = (Q_1 - Q_2)/(Q_1 + Q_2)$ along the longitudinal position of the crystal module, showing the capability to provide a position measurement.

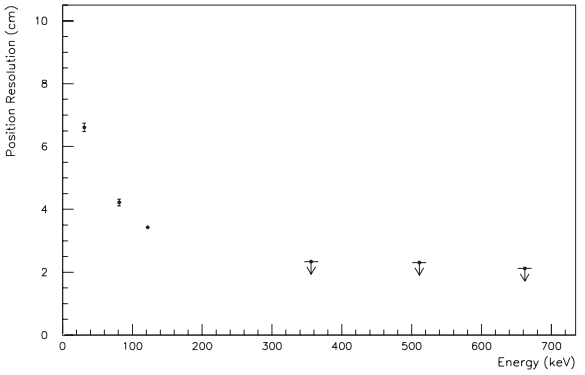

Fig. 7. The variation of longitudinal position resolution as a function of gamma energy, based on measurements with γ-sources at different energies. Limits are set for energy above 350 keV due to finite collimator size and the non-locationization of the multiple Compton scattering events.

Individual modules will be calibrated, both for the light yield and the light transmission profile, before installation. On the site, the stability of the crystals and PMTs can be monitored by radioactive sources illuminating the two end surfaces, as well as by cosmic-ray events. The stability of the electronics can be monitored with a precision pulse generation. LEDs placed at the end surface near the PMTs can be used to monitor stability of PMTs' response as well as the light transmission through the crystal.

The various potential experiments based on scintillating crystal detectors can essentially adopt a similar design. Much flexibility is available for optimization. Different modules can be made of different crystals. Different crystals can be glued together to form "phoswich" detectors in which cases the event location among the various crystals can be deduced from the different pulse shape. The passive target, as well as a different detector technology, can be inserted to replace a crystal module.

5. Background discussion

The background understanding is crucial in all low-background experiments. It is beyond the scope of this article to present a full discussion of the background and sensitivities for all the possible candidate crystals in the various potential applications listed in Section 3. In this section, we consider the key ingredients in the background issues relating to the CsI(Tl) experiment [25], followed by discussions of possible extensions to the lower-energy or smaller signal-rate experiments.

The experiment will operate at a shallow depth (about 30-m water-equivalent) near the reactor core, with the goal of achieving an 100 keV physics threshold corresponding to a $\bar{\nu}_e$–electron signal rate of O(1) per kg of CsI(Tl) per day [$\equiv$ "pkd"]. [5] As noted from the discussion in Section 2.3.3 and detector performance parameters achieved in Section 4, care should be taken and the standard procedures should be adopted for suppressing the ambient radioactivity background as well as those radioactivity from the equipment and surrounding materials. The dominant background channel is expected to be that of *internal* background from the CsI(Tl) itself. Based on prototype measurements, as well as detector and shielding

[5] For simplicity, we denote "*events per kg of CsI(Tl) per day*" by pkd in this section.

simulations, various contributions are summarized below.

(1) *Internal intrinsic radioactivity*: Fig. 3 and discussions in Section 2.3.6 demonstrate a ^{238}U and ^{232}Th concentration of less than 10^{-12} g/g level [$\sim$1 pkd], assuming that the decay chains are in equilibrium. In addition, direct counting method by a high-purity germanium detector shows ^{40}K and ^{137}Cs contaminations of less than 10^{-10} g/g [$\sim$1700 pkd] and 4×10^{-18} g/g [$\sim$1200 pkd] levels, respectively. Mass spectrometry method sets limits of ^{87}Rb to less than 8×10^{-9} g/g [$\sim$210 pkd] level.

(2) *Neutron capture*: The important channel comes from (n,γ) on ^{127}I producing ^{128}I ($\tau_{1/2} =$ 25 min, $Q = 2.14$ MeV). Ambient neutrons or those produced at lead shieldings have little probability of being captured by the CsI crystal target, being attenuated efficiently by the boron-loaded polyethylene. The neutron capture by the target are mostly due to cosmic-induced neutrons originating from the target itself, such that the ^{128}I production rate is about 1.8 pkd.

The other neutron-activated isotope, ^{134}Cs ($\tau_{1/2} = 2.05$ year, $Q = 2.06$ MeV), decays with 70% branching ratio by beta-decay (end point 658 keV), plus the emission of two γs (605 and 796 keV), and therefore will not give rise to a single hit at the low-energy region. The probability of producing single-hit at the 1.5–2 MeV region is suppressed by a factor of <0.05.

(3) *Muon capture*: Cosmic muons can be stopped by the target nuclei and subsequently captured [55–57]. The process will give rise to ^{133}Xe and ^{127}Te (<0.05 probability), both of which can lead to low-energy single-site background events. The expected rate is less than 1.5 pkd. The other daughter isotopes are stable.

(4) *Muon-induced nuclear dissociation*: Cosmic muons can disintegrate the target nuclei via the (γ,n) interactions or by spallations [58,59], at an estimated rate of $\sim$10 and $\sim$1 pkd, respectively. Among the various decay configurations of the final states nuclei of the (γ,n) processes, ^{132}Cs and ^{126}I, only about 20% (or $\sim$2 pkd) of the cases will give rise to low-energy single-hit background.

Therefore, the present studies place limits on internal radiopurity to the range of less than the 1000 pkd level. The effects due to cosmic-induced long-lived isotopes at this shallow depth but within elaborate shieldings are typically at the range of a few pkd. The residual background can be identified, measured and subtracted off by various means like alpha peaks, gamma peaks, and neutron-capture bursts. Such background subtraction strategies have been successfully used in accelerator neutrino experiments. For instance, the CHARM-II experiment measured about 2000 neutrino–electron scattering events from a sample of candidate events with a factor of 20 larger in size [60], achieving a few % uncertainty in the signal rate. A suppression factor of 100 is therefore a realistic goal.

In addition, one can use the conventional reactor ON/OFF subtraction to further enhance the sensitivities. Based on the above considerations, a residual background-to-signal ratio of less than 10 before reactor ON–OFF is attainable. In comparison, the best published limit on neutrino magnetic moment search with reactor neutrinos [61] is based on a Si(Li) target with a mass of 37.5 kg at a threshold of 600 keV and a reactor OFF/(ON–OFF) ratio of 120. Therefore, the CsI experiment should be able to achieve a better sensitivity in the studies of neutrino–electron scatterings.

The other applications typically allow the operation in underground sites so that the cosmic-induced background would be reduced compared to discussions above. The new challenges and complications are due to lower energy or smaller signal rates, discussed as follows:

(1) *Dark matter searches*: The present experimental background level [3–8] for the nuclear recoil energy range (10 keV and less) is around O(1) pkd per keV. This is comparable to the internal radiopurity limits already achieved in the CsI(Tl) prototype. However, the low energy (and therefore low light output) makes the the definition of a three-dimensional fiducial volume less efficient. The geometry and performance parameters of Fig. 4 is optimized for higher energy. Nevertheless, a simple variant of the concept can be adopted by using an active light guide based on crystals with distinguishably different time profiles as the target crystals. A possibility is the combination of pure CsI (decay time 10 ns) and CsI(Tl) (decay time

1000 ns). The location of the events can be obtained by pulse shape analysis. The rejection of PMT noise can be done also by PSD but will become delicate at the low energy (few photoelectrons) regime. The background subtraction procedures will require detailed knowledge of the effects from X-rays and Auger electrons at these low energies. The geometry of the crystal modules and the electronics design should be optimized to lower the detection and PSD threshold as far as possible. External shieldings should be optimized to minimize the effects of high energy neutrons, which can penetrate easily through the active veto to give the nuclear recoil background. Experiences from the operational NaI(Tl) detectors [3–8] can provide valuable input.

(2) *Solar neutrino experiments*: The energy range of interest (>100 keV) allows good detector performance for crystal scintillators. However, a much smaller $\nu_{\odot}$N–CC signal rate on the range of O(1) per 10 tons per day is expected. A target mass of tens of tons will be required, such that the scale-up schemes should be studied. A major R&D program, similar to the efforts with liquid scintillators [20] to enhance – and measure – the radiopurity level to 10^{-16} g/g range for U/Th is necessary, for any target isotopes and any detector technique. Still, the efforts can be focussed on to a single material, namely the crystal target itself. The radiopurity requirements can be relaxed for target isotopes, which can lead to distinct spatial and temporal signatures, such as ^{115}In [44–47] as well as ^{176}Yb, ^{160}Gd and ^{82}Se [49,50].

6. Outlook

Large water Cerenkov and liquid scintillator detectors have been successfully used in neutrino and astroparticle physics experiments. A new detector technology must be explored to open new windows of opportunities. Crystal scintillators may be well-suited to be adopted for low background experiments at the keV–MeV range. Pioneering efforts have already been made with NaI(Tl) crystals for dark matter searches, while another experiment with CsI(Tl) is being constructed to study low energy neutrino interactions. The present O(100 kg) target mass range can be scaled up to tens of tons, based on the successful experience of calorimeters in high energy physics experiments.

A generic detector design is considered in this article, demonstrating that defining a three-dimensional fiducial volume with minimal passive materials is possible. The large γ-attenuation at low energy can lead to a large suppression of background due to ambient radioactivity by the active veto layers. Consequently, the principal experimental challenges become focussed on the understanding, control and suppression of the radioactive contaminations in the crystals, as well as on the optimization of the detector design to realize an efficient, totally active, three-dimensional fiducial volume definition. The high γ-detection efficiency, good energy and spatial resolutions, low detection threshold, PSD capabilities and clean alpha signatures provide powerful diagnostic tools towards these ends.

There are still much room for research and development towards the realization of big experiments. Potential spin-offs in other areas are possible in the course of these efforts.

Acknowledgements

This work was supported by contracts NSC 87-2112-M-001-034 and NSC 88-2112-M-001-007 from the National Science Council, Taiwan.

References

[1] M. Ishii, M. Kobayashi, Prog. Crystal Growth Charact. 23 (1991) 245.
[2] G. Gratta, H. Newman, R.Y. Zhu, Ann. Rev. Nucl. Part. Sci. 44 (1994) 453.
[3] K. Fushimi, et al., Phys. Rev. C 47 (1993) R425.
[4] M.L. Sarsa, et al., Nucl. Phys. B 35 (1994) 154.
[5] N.J.C. Spooner, et al., Phys. Lett. B 321 (1994) 156.
[6] G. Gerbier, et al., Astropart. Phys. 11 (1999) 287.
[7] R. Bernabei, et al., Phys. Lett. B 389 (1996) 757.
[8] R. Bernabei, et al., Phys. Lett. B 450 (1999) 448.
[9] H. Grassman, E. Lorentz, H.G. Moser, Nucl. Instrum. Methods 228 (1985) 323.
[10] P. Schotanus, R. Kamermans, P. Dorenbos, IEEE Trans. Nucl. Sci. 37 (1990) 177.

[11] E. Storm, H.I. Israel, Nucl. Data Tables A 7 (1970) 565.
[12] R. Chipaux, et al., IEEE Trans. Nucl. Sci. 46 (1999) 531.
[13] P. Jagam, J.J. Simpson, Nucl. Instrum. Methods A 324 (1993) 389.
[14] J. Alarja, et al., Nucl. Instrum. Methods A 242 (1986) 352.
[15] P. Kreutz, et al., Nucl. Instrum. Methods A 260 (1987) 120.
[16] C.L. Morris, et al., Nucl. Instrum. Methods 137 (1976) 397.
[17] M.S. Zucker, N. Tsoupas, Nucl. Instrum. Methods A 299 (1990) 281.
[18] U. Kilgus, R. Kotthaus, E. Lange, Nucl. Instrum. Methods A 297 (1990) 425.
[19] R. Kotthaus, Nucl. Instrum. Methods A 329 (1993) 433.
[20] G. Alimonti, et al., Nucl. Instrum. Methods A 406 (1998) 411.
[21] P. Vogel, J. Engel, Phys. Rev. D 39 (1989) 3378.
[22] B. Kayser, et al., Phys. Rev. D 20 (1979) 87.
[23] C. Broggini, et al., Nucl. Instrum. Methods A 311 (1992) 319.
[24] C. Amsler, et al., Nucl. Instrum. Methods A 396 (1997) 115.
[25] H.T. Wong, J. Li, Nucl. Phys. B (Proc. Suppl.) 77 (1999) 177.
[26] R. Barabanov, et al., Astropart. Phys. 5 (1996) 159.
[27] B. Armbruster, et al., Phys. Lett. B 423 (1998) 15.
[28] H.C. Lee, Nucl. Phys. A 294 (1978) 473.
[29] T.W. Donnelly, R.D. Peccei, Phys. Rep. 50 (1979) 1.
[30] T. Suzuki, Y. Kohyama, K. Yazaki, Phys. Lett. B 252 (1990) 323.
[31] J. Bernabeú, et al., Nucl. Phys. B 378 (1992) 131.
[32] K. Kubodera, S. Nozawa, Int. J. Mod. Phys. E 3 (1994) 101.
[33] B. Sadoulet, Nucl. Phys. B (Proc. Suppl.) 77 (1999) 389.
[34] J. Ellis, R.A. Flores, J.D. Lewin, Phys. Lett. B 212 (1988) 375.
[35] J. Ellis, R.A. Flores, Phys. Lett. B 263 (1991) 259.
[36] C. Bacci, et al., Astropart. Phys. 2 (1994) 117.
[37] R. Hazama, Thesis, Osaka University, 1998.
[38] S. Pecourt, et al., Astropart. Phys. 11 (1999) 457.
[39] H. Ejiri, K. Fushimi, H. Ohsumi, Phys. Lett. B 317 (1993) 14.
[40] P. Belli, et al., Phys. Lett. B 387 (1996) 222.
[41] M.W. Goodman, E. Witten, Phys. Rev. D 31 (1985) 3059.
[42] J. Ellis, R.A. Flores, J.D. Lewin, Phys. Lett. B 212 (1988) 375.
[43] R.E. Lanou Jr., Nucl. Phys. B (Proc. Suppl.) 77 (1999) 55.
[44] R.S. Raghavan, Phys. Rev. Lett. 37 (1976) 259.
[45] L. Gonzalez-Mestres, D. Perret-Gallix, Nucl. Instrum. Methods A 279 (1989) 382.
[46] J.P. Chaminade, et al., J. Cryst. Growth 99 (1990) 799.
[47] M. Avenier, et al., Nucl. Phys. B (Proc. Suppl.) 28A (1992) 496.
[48] C.C. Chang, C.Y. Chang, G. Collins, Nucl. Phys. B (Proc. Suppl.) 35 (1994) 464.
[49] R.S. Raghavan, Phys. Rev. Lett. 78 (1997) 3618.
[50] LENS Letter of Intent, 1999.
[51] A. Morales., Nucl. Phys. B (Proc. Suppl.) 77 (1999) 335.
[52] A. Danevich, et al., Phys. Lett. B 344 (1995) 72.
[53] S.F. Burachas, et al., Phys. Atom. Nucl. 58 (1995) 153.
[54] M. Kobayashi, S. Kobayashi, Nucl. Phys. A 586 (1995) 457.
[55] S. Charalambus, Nucl. Phys. A 166 (1971) 145.
[56] T. Suzuki, D.F. Measday, J.P. Roalsvig, Phys. Rev. C 35 (1987) 2212.
[57] T. Kozlowski, et al., Nucl. Phys. A 436 (1985) 717.
[58] G. Cocconi, V. Cocconi Tongiorgi, Phys. Rev. 84 (1951) 29.
[59] S. Hayakawa, Phys. Rev. 84 (1951) 37.
[60] P. Vilain, et al., Phys. Lett. B 335 (1994) 246.
[61] A.I. Derbin, et al., JETP Lett. 57 (1993) 769.